Droplet Retention and Shedding on Slippery Substrates

Bethany Orme, Glen McHale, Rodrigo Andres Ledesma-Aguilar, and Gary George Wells

Langmuir, **Just Accepted Manuscript** • DOI: 10.1021/acs.langmuir.9b00931 • Publication Date (Web): 19 Jun 2019

Droplet Retention and Shedding on Slippery Substrates

Bethany V. Orme, Glen McHale, Rodrigo Ledesma-Aguilar and Gary G. Wells

Smart Materials & Surfaces Laboratory,

Faculty of Engineering & Environment, Northumbria University,

Newcastle upon Tyne, NE1 8ST, UK

Abstract

A significant limitation for droplet mobility on solid surfaces is to overcome the inherent pinning of the droplet's contact line that occurs due to chemical/physical heterogeneities. A recent innovation is to use surface texture or porosity to create a stabilised lubricant surface. Droplets on such Slippery Liquid Infused Porous Surfaces/Lubricant Impregnated Surfaces (SLIPS/LIS) are highly mobile due to the lubricant layer. Low pinning of the contact line reduces the energy required to move a droplet, however, it makes it difficult to accurately position the droplet or to stop its motion altogether. In this paper, a simple structure (step), as small as a few microns in height, is used to introduce controlled droplet pinning on a slippery substrate. The key effect is identified as the capillary force, arising from the interaction between the lubricant menisci created by the step and droplet. The effect of changing step height, lubricant thickness and initial position on step-droplet interactions has been investigated, showing droplets can both be repelled from and attracted to the step. To measure the adhesion strength, we report droplet detachment angle measurements under gravity, and scaling of force with lubricant thickness/step height ratio. Under certain conditions, the interaction strength is sufficient to ensure droplet-step attachment even when the surface is rotated to an upside-down orientation. These findings presented can motivate the design of SLIPS structures, capable of shedding or retaining droplets preferentially, e.g., according to size or wettability, relevant to applications from microfluidics to fog harvesting.

Keywords: Slippery Liquid-Infused Porous Surface, SLIPS, Lubricant Impreganted Surface, droplets, Cheerios Effect, wetting ridge, low pinning, wettability, menisci.

Corresponding Author: gary.wells@northumbria.ac.uk

Introduction

The ability to accurately position a droplet on a surface has relevance in a variety of industrial and practical applications, such as inkjet printing[1], self-cleaning surfaces[2], precise deposition of particles[3,4], microfluidics[5], drug delivery[6] and cell analysis[7].

Recent research into surface design has focused on supressing[8,9], and in some cases eliminating, droplet pinning to create freely-moving contact lines[10,11]. This increases the ease with which a droplet can be transported by reducing the frictional force created by the droplet's direct contact with the underlying substrate[12]. The reduction of this frictional force has previously been achieved using superhydrophobic surfaces which reduce the solid-liquid contact area[13–15], creating a Cassie-Baxter[16,17] condition, or by chemical treatments such as Teflon[18]. Low pinning has been most successfully achieved by producing Slippery Liquid Infused Porous Surfaces or Liquid Impregnated Surfaces (SLIPS/LIS) which are inspired by the Nepenthes pitcher plant[19] and based on an imbibed lubricant layer[20].

However, SLIPS/LIS lack the ability to accurately control the position of a droplet. Previous attempts to overcome this barrier include introducing an "on/off switch" to the SLIPS properties via thermal actuation[21], but controlling the droplet in the SLIPS phase is difficult.

Accidental surface defects on a SLIPS/LIS can pin droplets into fixed, stationary positions and can be attributed to large increases in droplet sliding angles. Drawing inspiration from this idea, the forces created by tailor made small-scale structures on an otherwise slippery surface could be implemented as a method for droplet positioning and control. Since any surface defect, or any droplet on a SLIP surface, creates a deformation in the meniscus of the lubricating liquid, it is expected that capillary forces arise between a droplet and a surface defect even in the absence of direct droplet/solid contact[22].This is similar to the Cheerios Effect[23] and responsible for the attractive interactions between floating solid objects or bubbles mediated by liquid-gas menisci. A similar effect has also been seen for droplets on soft, elastic solids where the thickness of the layer and conservation of volume determines whether the force is attractive or repulsive[24].

Recently, Guan *et al.* showed aspects of the Cheerios Effect on a SLIPS coated macrostructure, in the form of a V-shaped channel. This was used to accurately guide and position a droplet[25].In this case the lubricating liquid layer was mobile and able to fully cloak the droplet due to a positive spreading coefficient[10,22]. The wetting ridge at the channel wall and the wetting ridge around the base of the droplet both have the same sign of curvature, leading to an overall attractive capillary force[23]. However, the Cheerios effect for particles on liquid surfaces can also create repulsive capillary forces using menisci, or wetting ridges, with curvature of opposite signs[24].

Despite these previous attempts to introduce accurate droplet positioning to surfaces, controlling the droplet on a SLIPS/LIS remains an open challenge. In this paper, experiments are reported that show how a structure, a step as small as 7 µm in height, treated with an easy to apply SLIPS coating[26] is capable of producing attractive and repulsive forces on a droplet in a reproducible manner. The mechanism is controlled purely by capillary forces arising from the combination of the droplets meniscus, which forms wetting ridges with positive curvature (where the meniscus rises above the plane of the interface)[27] and the positive meniscus created by the solid step. The strength of the attractive interaction is characterised by measuring the detachment angle of droplets as a function of step height, oil thickness and initial droplet deposition position relative to the step. A scaling relation for this force in terms of the ratio of height of the step to oil thickness is reported.

Method

Figures 1a and 1b show the step sample preparation method. Glass slides/wafers were used as a substrate base onto which a step was attached *via* two different methods. In Method 1, a rectangular

Glass Cover Slip was attached to the top of a 25mm × 75mm borosilicate, glass microscope slide. This method created a sharp, vertical step with a fixed height of 140 μm.

Method 2 was used to create steps of variable heights. Standard photolithographic techniques were used to apply at layer of negative photoresist, SU-8 (Microchem, SU-8 2010, 2050 and 2100). The thickness of the layer was varied in the range of 7 μm to 150 μm by changing the viscosity and spin speed. The exposure time was varied in accordance with the SU-8 thickness. The heights of the resulting SU-8 steps were measured using white-light optical profilometry (Bruker Contour GT).

Figures 1c and 1d depict the process of coating the steps with a thin SLIPS layer. First, a nanoparticle and solvent-based coating (Glaco Mirror Coat) was sprayed onto the samples to create a uniform thickness, porous hydrophobic coating[26] (Figure 1c). The nanoparticle layered samples were then infused with a lubricating layer of Silicone Oil (surface tension, γ=19.8 mN m^{-1} and viscosity, η=19 mPa s) by automated dip coating (Fisnar F4200N). The automation allowed for controllable sample withdrawal from a silicone oil bath, with the withdrawal speed, V, varied within the range of 0.1 mm s^{-1} to 2.5 mm s^{-1}. This corresponds to the thickness of the oil layer, h_o, shown in Figure 1d.

To calibrate the relationship between the thickness of the oil layer, h_o, and the withdrawal speed, the apparent thickness of the oil layer was measured using reflectometry (Filmetrics F20) and the refractive index of silicone oil, 1.403. The experimental results are reported in Figure 1e (black circles), and are well fitted by the Landau Levich-Derjaguin (LLD)[28,29] equation (Figure 1e, solid red line), $h_o \approx 0.94\, a\, Ca^{2/3}$, where a is the capillary length of the oil (≈ 1.46 mm) and Ca the capillary number ($Ca = \eta\, V/\gamma$).

During the dip coating procedure, the oil fully coats the particles to create index matched layers and renders the porous nano-particle layer transparent, therefore the value measured by reflectometry is the combination of the two layers. The uniformity and thickness of the dry nanoparticle layer was measured *via* cross-sectional SEM scans of several samples (Tescan MIRA3). Figure 1e inset, shows a typical SEM scan of the nanoparticle layer. The average thickness of the nanoparticle layer was determined to be 1.93 ± 0.16 μm. The thickness of the mobile oil layer was determined by subtracting the thickness of the nano-particle layer from the apparent thickness measured by reflectometry (shown as the grey dotted line in Figure 1e). Whilst it is expected there will be some oil drainage of the mobile oil layer, on the experimental timescale the greatest percentage oil weight loss (from the thickest oil sample, h_o= 24.79 μm) is only 2.72%.

The thickness of the mobile layer is the determining factor when considering the angle formed when the droplet is in contact with the surface. For the SLIP surfaces produced in these experiments it is assumed there is no direct solid/droplet contact due to the reduction in contact angle hysteresis between a dry surface and one that has been infused with an oil layer. For the dry surface the hysteresis is measured to be 7.5° ± 0.5° and when lubricated 0.56° ± 0.20°. Even for a surface with a thermodynamically stable lubricating layer of thickness equivalent to the particle layer, the contact angle hysteresis is still lower than the dry surface at 3.4° ± 0.2°. Despite the lack of direct contact, the water droplet and oil layer still form an angle determined by the interfacial tensions and given by the Neumann triangle[30]. For a thin oil layer, there is only a small availability of oil, creating a small wetting ridge and apparent contact angle ≈ 100°. As the oil layer is increased the wetting ridge grows and the apparent contact angle decreases[31].

To determine whether it is more energetically favourable to have a water droplet that will be fully cloaked with the lubricating liquid or an uncloaked water droplet a simple spreading coefficient calculation can be completed for the combination of liquids used within this system. To be cloaked the interfacial tension for water/vapour ($\gamma_{w,v}$) must be greater than the combination of the water/oil and oil/vapour interfaces ($\gamma_{w,o} + \gamma_{o,v}$), meaning the spreading parameter must be positive

$$S^{v}_{w,o} = \gamma_{w,v} - \gamma_{w,o} - \gamma_{o,v} \geq 0. \quad (1)$$

By using $\gamma_{w,v} =$ 72.8 mN m^{-1}, $\gamma_{w,o} =$ 38 mN m^{-1} [32] and $\gamma_{o,v} =$ 19.8 mN m^{-1} [31] the spreading parameter is calculated to be 15.8 mN m^{-1}, therefore the water droplet will be fully cloaked by the oil.

To characterise the static friction acting on a droplet on the slippery surfaces, the sliding angle of multiple droplets has been measured. In this instance the sliding angle, φ_s, is defined as the threshold angle for which the surface must be inclined to induce the onset of constant droplet motion. Water droplets of 2 µl were used to ensure that the droplet diameter was below the capillary length, thus maintaining a spherical cap and ruling out gravitational effects on the droplet shape. Each sample was placed on the tilting stage of a Kruss DSA30 Contact Angle Meter and a droplet placed onto the step. The sample was then tilted in a direction parallel to the step until motion was observed. The average sliding angle was measured to be 0.56° ± 0.20°.

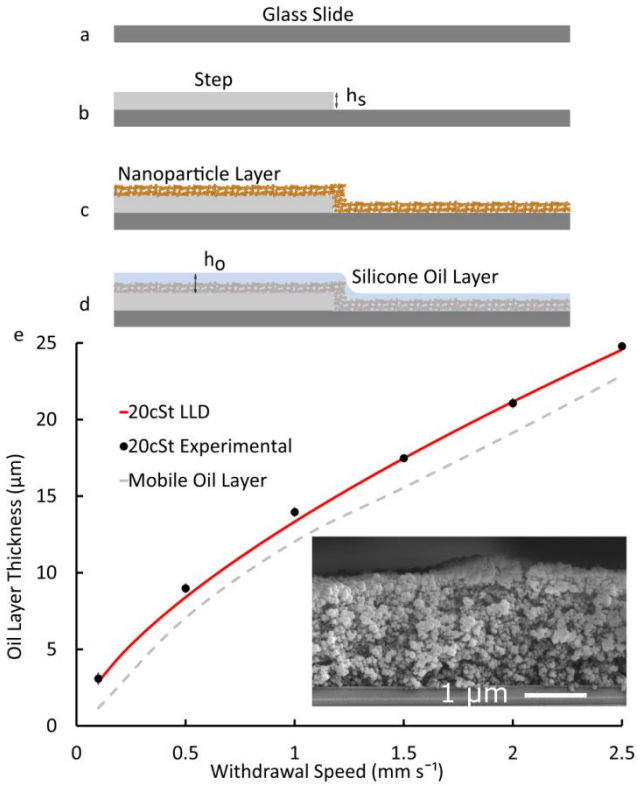

***Figure 1**: Sample production and characterisation. **a-d** Schematic of the production of the step from, a glass cover slip and SU-8 (via simple photolithography), where h_s is varied and measured by white-light optical profilometry. The nanoparticle coating consists of a commercial product (Glaco) and applied via spray coating. Silicone oil imbibition is performed by a dip coating method where the withdrawal speed can be varied to produce different oil layer thicknesses. **e** SEM image of a typical sample cross section, indicating the uniformity of the coating and nanoparticle layer height. **f** Oil thickness for different withdrawal speeds. Black dots are the experimental layer thickness measured using a reflectometer. Red solid line is a fit to the LLD equation. Grey dashed line indicates the estimated oil layer thickness.*

Results and Discussion

Step adhesion force

To measure the adhesion force of the step, droplets of volume 2 µl were placed below a step coated in a layer of silicone oil. The initial inclination of the sample was 0°, with the sample horizontal, so no external forces acted on the droplets. The droplets were immediately attracted to the step, suggesting an unbalanced capillary force created by the interaction between the wetting ridges produced by both

the step and the droplet. Figure 2a shows a schematic of the system and the positioning of the water droplet in relation to the step. Once the droplet had settled in a static position, the sample was tilted in a direction normal to the step where gravity pulled the droplet away from the step. The angle of tilt was changed in increments of 0.20°. Figure 2b shows the side profiles of the droplets throughout the tilting process. The last image in the sequence shows the droplet at the point of detachment. On a 7 um SU-8 step coated in a 3.09 um layer of silicone oil the sliding or detachment angle, φ_s, occurred at φ_s = 7.10° ± 0.20°, which is one order of magnitude larger than the sliding angle measured on a flat surface. The experiment was repeated across several samples, with 5 droplets deposited onto each separate sample to ensure the adhesion force was only being governed by the step. The average detachment angle obtained 7.18° ± 0.31°.

Changing the step height to a maximum of 150 µm leads to similar observations, albeit with a substantially larger average detachment angle of 46.22° ± 1.63°. The droplet itself maintains a spherical cap, however, it can be seen that there is now a very clear asymmetry between the right-hand side wetting ridge (leading ridge) and the left-hand side (trailing ridge) (Figure 2b, bottom row), indicating the presence of a capillary force balancing the driving force of gravity. When comparing the top and bottom row images in Figure 2b as well the enlarged image of the wetting ridge for the 7 µm step height (Figure 2c), it is clear that the larger step height (150 µm) produces the larger wetting ridge, indicating a greater oil availability. This is likely due to the droplet drawing oil into the ridge along the filled corner of the step and not from the thin film of oil. Since the curvature of the wetting ridge is weaker at the leading droplet edge of the than that of the trailing droplet edge, a higher pressure is expected at the front of the droplet. This disparity enables the droplet to remain stuck to the step with a flow of lubricating liquid through the ridge from leading to trailing, balancing the gravitational force. Hence, the stronger capillary force (due to the larger difference in ridge curvature) explains the significantly higher detachment angle.

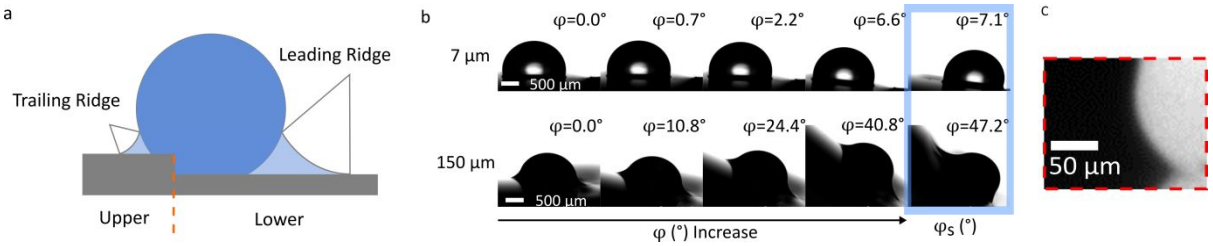

Figure 2*: Changes in position and configuration of droplets by varying step height (h_s) and the effect this has on detachment angle (φ_s).* ***a*** *A schematic showing how a water droplet interacts with the system with the upper and lower sections designated on the sample and the asymmetry between trailing and leading wetting ridges defined.* ***b*** *Sequence of images showing the droplet shape evolution during sample tilting, step detachment and finally droplet motion as h_s increases.* ***c*** *In the dashed red box, there is an image at 10 times zoom to depict more clearly the smallest wetting ridge achievable on the thinnest oil layer (h_o= 3.09 µm).*

Figure 3a shows the variation of the detachment angle as a function of the step height, h_s on substrates coated with different thickness of the oil layer. The data shows a linear increase of φ_s with $h_s$which holds regardless of the material used to create the step (glass or SU-8). For a given step height, however, increasing the thickness of the oil layer has the effect of reducing the detachment angle (Figure 3a - black and red markers). To examine the effect of increasing the thickness of the oil layer in more detail, experiments in the range of $h_o \approx$ 3-25 µm were carried out. The data for h_s=140 µm confirms a decrease in the detachment angle with increasing oil layer thickness (coloured triangles in Figure 3a). Such a reduction on the adhesion force is likely due to a reduction in the difference in curvature of the leading and trailing ridges caused by the restriction to the shape of the wetting ridge imposed by the thickness of the oil layer. This concept was examined in Semprebon *et al.*[33] where the droplet is seen to deform more as the wetting ridge pressure increases, which is equivalent to decreasing the oil layer thickness. The combination of the two length scales, oil thickness and step height, used in this experiment appears to show an approach to saturation at ≈ 12° for the largest

values of oil thickness (h_o= 21.07 µm and 24.79 µm). Therefore the adhesion force at the detachment angle (φ_s), is expected to be the capillary force, F_{cap}, balanced by the gravitational force, F_g, acting on the droplet. Due to the fact the droplet is stationary any viscous drag effects are ignored. Since $F_g \sim \sin \varphi_s$, then $F_{cap} \sim \sin \varphi_s$. The dependence of $\sin \varphi_s$ on the step height and the thickness of the oil layer is shown in Figure 3b. As h_s controls the geometry of the step and h_o the length scale of the oil meniscus, it is reasonable to assume the force is dependent on the ratio h_s/h_o. As shown in Figure 3b, a plot of $\sin \varphi_s$ vs (h_s/h_o) leads to a collapse of the data onto a single curve, which appears to fit a power-law in the form $F_{cap} \sim \left(h_s/h_o\right)^{1/2}$.

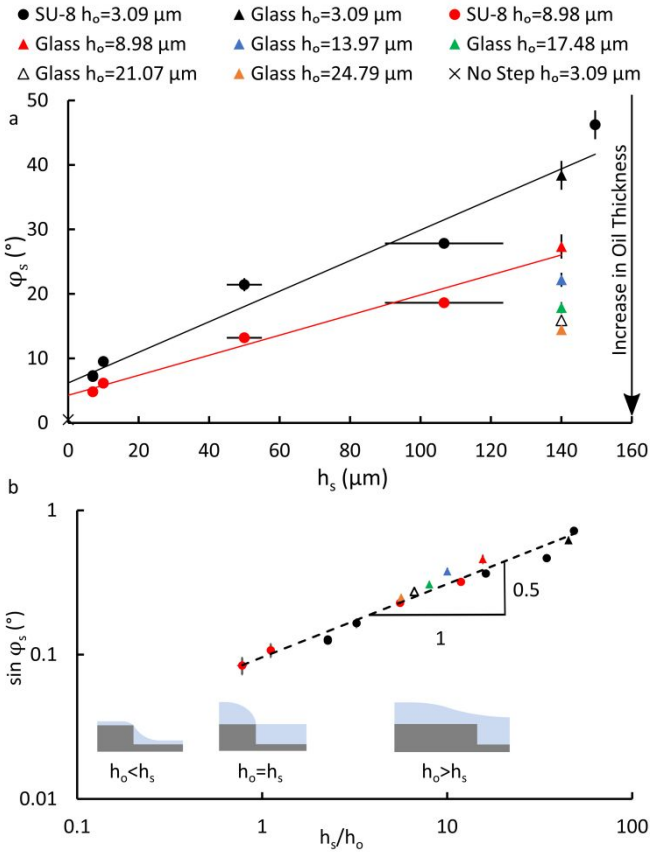

***Figure 3**: Effect on detachment angle (φ_s) as step height (h_s) increases. **a** Detachment angle (φ_s) data for increasing step heights (black circles and black triangle) for the thinnest oil layer (3.09 µm). Red circles and red triangle show the reduction of φ_s for a thicker oil layer. All triangles indicate the evolution of φ_s from minimum to maximum oil thickness. Each of the data points corresponds to an average of five experimental results. **b** Data from **a** plotted on a log-log scale with accompanying oil layer schematics. $\sin \varphi_s$ scales as the square root of the ratio of step height to oil thickness.*

Effect of the initial position of the droplet relative to the step

By splitting the step into 2 distinct sample sections, upper and lower, the initial droplet deposition position was investigated. The upper section is that seen at the top of the step, the lower section is the portion of the sample below the step (Figure 2a).

2 µl droplets were placed onto the upper section of a 140 µm step for different oil thicknesses. On deposition, droplet repulsion from the step can be seen. As the lubricant layer is expected to be pinned to the step corner[34] a meniscus of negative curvature is formed at the corner (where the meniscus curves below the interface)[27]. Therefore, there is a combination of menisci of opposite curvatures, hence the repulsion can be explained.

Tilting the sample clockwise, so that gravity forces the droplet towards the step leads to a two-stage process before the droplet is finally detached and slides down the surface. Firstly, for a range of tilting angles, the droplet remains above the step due to the repulsive force. During this stage, the leading-edge wetting ridge continues to grow until a tilting angle where the drop overcomes the corner and moves to the lower section of the step. At this point, the attractive force acts, adhering the droplet to the step, retaining the droplet on the surface in a stationary position. Further tilting is required until the droplet fully detaches and slides down. As shown in Figure 4a, this final detachment angle is consistently below the values measured for droplets initially placed on the lower sample section, this becomes more prominent for thinner oil layers. Therefore, the droplets exhibit a different behaviour depending on the initial conditions of the experiment.

A possible mechanism for this effect is the relaxation that the droplets undergo in the two different initial positions. A droplet initially placed on the lower section is only subject to the capillary force formed by the droplet and step wetting ridges, pulling the droplet into a stationary position, adhered to the step. However, for a droplet initially placed on the upper section, the transition to the lower stationary position occurs under the two opposing forces of gravity and capillary force. Therefore, the difference between these forces reduces the step adhesion force. Indeed, the top-view images of the droplets presented in Figures 4b and 4c confirm that the contact between the step and droplet changes, depending on the initial droplet deposition position. When arriving from the upper section (Figure 4b), the droplet is deformed slightly by the step, with the trailing edge becoming flattened. However, the droplet itself does not appear to be in contact with the step and has, in fact, a droplet-step separation of 54.45 µm ± 1.66 µm. When arriving to the step from the lower section (Figure 4c), both the wetting ridge and droplet are attached to the step giving an average droplet-step overlap of 88.34 µm ± 1.66 µm. This difference in configuration is the most likely cause for the observed difference in the detachment angles between the two initial conditions.

What is also noticeable is the reduction in the difference between the detachment angle in the 2 configurations as h_o is increased. This can be attributed to the difference in droplet/wetting ridge contact area on the step. For thin oil layers the difference between having both the droplet and wetting ridge attached to the step and just the wetting ridge is large due to the small size of the wetting ridge and equates to a large difference in the force required to detach the droplets. However, with a larger wetting ridge changing between purely wetting ridge attachment and both droplet and wetting ridge attachment leads to a small overall change in contact area and therefore a small change in force required to detach the droplet.

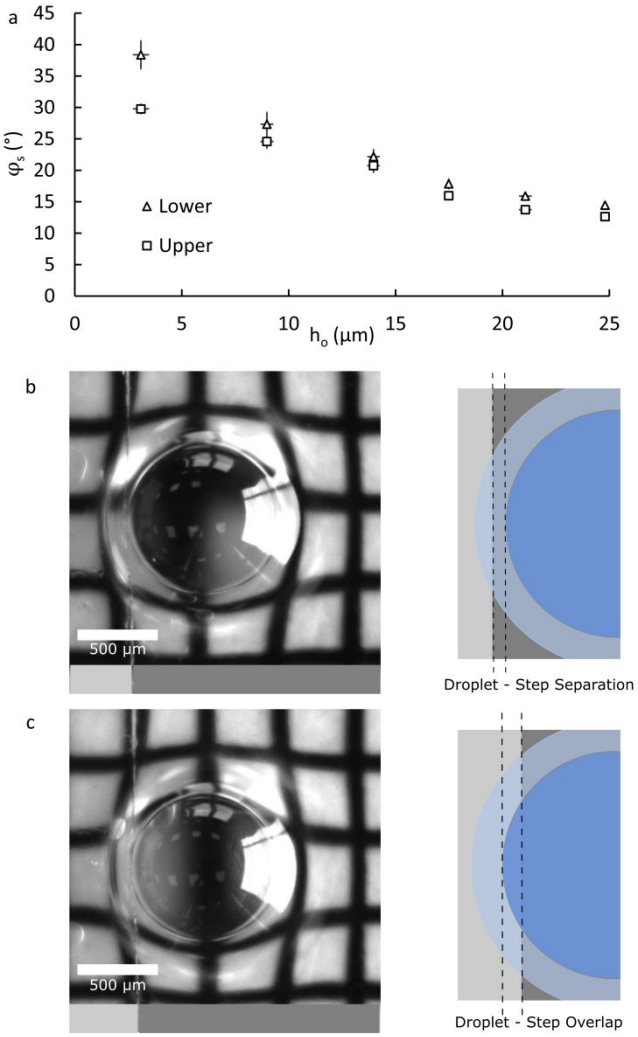

Figure 4*: Exact droplet positions when droplet has arrived at its final stationary point on the stepped samples, close to the point of detachment, given differing initial positions.* ***a*** *Detachment angles for 140 µm hs with increasing oil layer thickness. Squares initial position on the step's upper portion, triangles on the lower, both tilted in a clockwise direction (away from the step).* ***b*** *Top view of 2 µl droplet close to step detachment, with its initial position having been on the upper portion of the step, along with a schematic to show the droplets separation from the step.* ***c*** *2 µl droplet close to step detachment where the droplets initial position was on the lower portion of the stepped sample. The accompanying schematic indicates the droplets overlap with the step.*

Effect of the tilting direction

To investigate the full range the interactions between droplets and steps, a set of experiments was conducted where the substrate was tilted in the opposite, negative direction (clockwise) and the droplets start on the same upper/lower sample sections previously defined. In these experiments, a droplet initially on the lower surface must now climb the step before being detached from the surface and a droplet on the upper surface must simply move away from the step. Figure 5 shows measurements for all four of the possible configurations. Figure 4a and 4b above the 0° axis show the data we have previously discussed.

Remarkably, for droplets that must climb the step coated in thin oil layers, the sample can undergo a full 180° rotation whilst still retaining the droplet (indicated by the crosses in Figure 5a). The final sample position results in an upside-down orientation of the droplet. If the rotation was to continue, the droplet will transition from its original configuration (droplet deposited below the step and tilted anticlockwise) to the configuration seen on the upper, positive axis of Figure 5a.

As previously mentioned, a droplet placed above the step is initially repelled from the step before again becoming stationary away from the effects of the oil curvatures. Hence, it is expected that the angle required for droplets to move away from the top of the step matches the sliding angle on a perfectly flat SLIPS (in this case 0.56° ± 0.20°). This is indeed the case, as shown by filled triangles in Figure 5b.

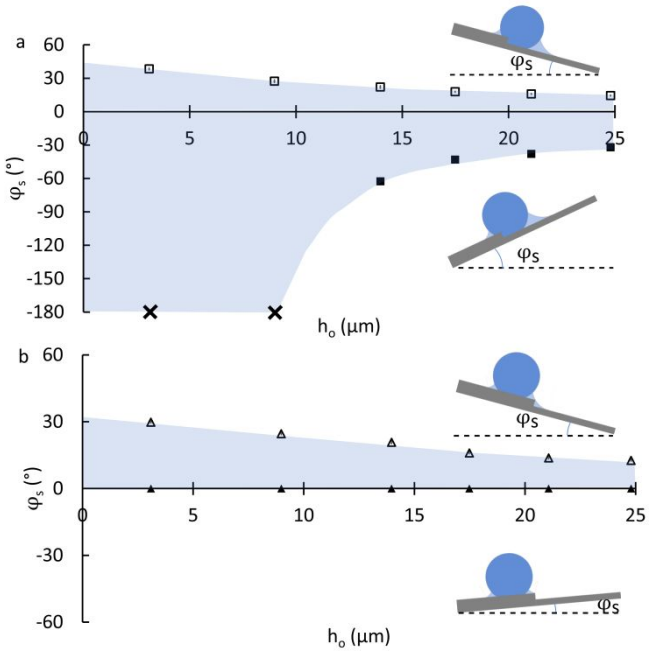

Figure 5*: Changes in droplets initial position and direction of tilt (clockwise/anticlockwise).* ***a*** *Comparison between 2 μl droplets placed on the lower portion of the step and tilted both clockwise and anticlockwise for increasing oil thickness. Shaded area indicates where the droplet is stationary on the surface and stuck to the step. The (crosses) indicate droplets that did not slide at all on the surface and remained there even at 180°.* ***b*** *2 μl droplet placed on the upper portion of the step and the same procedure as seen in* ***a*** *applied. The error bars on both graphs are equivalent to the size of the symbols and each data point corresponds to an average of results from 5 experiments.*

Conclusions

In this study, the interaction between water droplets and a SLIPS/LIS coated macroscopic, linear step has been investigated, with a view to improving control in droplet retention and shedding. The effect of the step is to induce the formation of a meniscus of the SLIPS/LIS lubricant layer, which leads to capillary interactions with the meniscus of the lubricant layer induced by a droplet. Droplets are attracted to the lower face of a step whilst they are repelled from the top edge of the step in a manner consistent with the Cheerios effect. The capillary force exerted on a droplet by the lower side of a step has been characterised by measuring the detachment angle in the presence of gravity for different step heights/oil-layers and found that, for the range of measurements considered in our experiments this force scales as $F_{cap} \sim (h_s/h_o)^{1/2}$. Whilst the theoretical model for why F_{cap} scales to the half power is still unclear it is a subject that requires further investigation. It has also been shown that the capillary force depends on the initial position of the droplet relative to the step. A droplet approaching from the upper section of a step experiences a lower adhesion force due to the effect of gravity, creating a lower detachment angle and a "memory" of the initial conditions. Finally, we have shown that droplets forced against a step due to gravity can sustain tilting angles up to 180° without detaching from the surface. The simple step configuration reported in this paper is an illustration of how capillary interactions mediated by the lubricant layer of SLIPS/LIS can provide a means for droplet retention and shedding. We believe that our results can motivate the study of more complex features as a means

to achieve better control on the transport and location of droplets on low-friction surfaces by exploiting the capillary interactions presented here.

Acknowledgement

BVO acknowledges the University of Northumbria at Newcastle for its support via a postgraduate research studentship. The authors would like to thank Dr. Andrew Edwards for assistance during sample production.

References

(1) Singh, M.; Haverinen, H. M.; Dhagat, P.; Jabbour, G. E. Inkjet Printing-Process and Its Applications. *Adv. Mater.* **2010**, *22* (6), 673–685.
(2) Quéré, D. Wetting and Roughness. *Annu. Rev. Mater. Res.* **2008**, *38* (1), 71–99.
(3) Deegan, R. D.; Bakajin, O.; Dupont, T. F.; Huber, G.; Nagel, S. R.; Witten, T. A. Capillary Flow as the Cause of Ring Stains from Dried Liquid Drops. *Nature* **1997**, *389* (6653), 827–829.
(4) Yunker, P. J.; Still, T.; Lohr, M. A.; Yodh, A. G. Suppression of the Coffee-Ring Effect by Shape-Dependent Capillary Interactions. *Nature* **2011**, *476* (7360), 308–311.
(5) Baroud, C. N.; Gallaire, F.; Dangla, R. Dynamics of Microfluidic Droplets. *Lab Chip* **2010**, *10* (16), 2032–2045.
(6) Leslie, D. C.; Waterhouse, A.; Berthet, J. B.; Valentin, T. M.; Watters, A. L.; Jain, A.; Kim, P.; Hatton, B. D.; Nedder, A.; Donovan, K.; et al. A Bioinspired Omniphobic Surface Coating on Medical Devices Prevents Thrombosis and Biofouling. *Nat. Biotechnol.* **2014**, *32* (11), 1134–1140.
(7) Ling, S.; Luo, Y.; Luan, L.; Wang, Z.; Wu, T. Inkjet Printing of Patterned Ultra-Slippery Surfaces for Planar Droplet Manipulation. *Sensors Actuators, B Chem.* **2016**, *235*, 732–738.
(8) McHale, G.; Shirtcliffe, N. J.; Newton, M. I. Contact-Angle Hysteresis on Super-Hydrophobic Surfaces. *Langmuir* **2004**, *20* (23), 10146–10149.
(9) Wu, C. J.; Li, Y. F.; Woon, W. Y.; Sheng, Y. J.; Tsao, H. K. Contact Angle Hysteresis on Graphene Surfaces and Hysteresis-Free Behavior on Oil-Infused Graphite Surfaces. *Appl. Surf. Sci.* **2016**, *385*, 153–161.
(10) Guan, J. H.; Wells, G. G.; Xu, B.; McHale, G.; Wood, D.; Martin, J.; Stuart-Cole, S. Evaporation of Sessile Droplets on Slippery Liquid-Infused Porous Surfaces (SLIPS). *Langmuir* **2015**, *31* (43), 11781–11789.
(11) Wang, L.; McCarthy, T. J. Covalently Attached Liquids: Instant Omniphobic Surfaces with Unprecedented Repellency. *Angew. Chemie - Int. Ed.* **2016**, *55* (1), 244–248.
(12) Hancock, M. J.; Sekeroglu, K.; Demirel, M. C. Bioinspired Directional Surfaces for Adhesion, Wetting, and Transport. *Adv. Funct. Mater.* **2012**, *22* (11), 2223–2234.
(13) Kota, A. K.; Li, Y.; Mabry, J. M.; Tuteja, A. Hierarchically Structured Superoleophobic Surfaces with Ultralow Contact Angle Hysteresis. *Adv. Mater.* **2012**, *24* (43), 5838–5843.
(14) Shirtcliffe, N. J.; Aqil, S.; Evans, C.; McHale, G.; Newton, M. I.; Perry, C. C.; Roach, P. The Use of High Aspect Ratio Photoresist (SU-8) for Super-Hydrophobic Pattern Prototyping. *J. Micromechanics Microengineering* **2004**, *14* (10), 1384–1389.
(15) Shirtcliffe, N. J.; McHale, G.; Atherton, S.; Newton, M. I. An Introduction to Superhydrophobicity. *Adv. Colloid Interface Sci.* **2010**, *161* (1–2), 124–138.
(16) Cassie, A. B. D.; Baxter, S. Wettability of Porous Surfaces. *Trans. Faraday Soc.* **1944**, *40* (5), 546–551.
(17) Barthlott, W.; Neinhuis, C. Purity of the Sacred Lotus, or Escape from Contamination in Biological Surfaces. *Planta* **1997**, *202* (1), 1–8.
(18) Simpson, J. T.; Hunter, S. R.; Aytug, T. Superhydrophobic Materials and Coatings: A Review. *Reports Prog. Phys.* **2015**, *78* (8), 86501.
(19) Bauer, U.; Federle, W. The Insect-Trapping Rim of Nepenthes Pitchers: Surface Structure and Function. *Plant Signal. Behav.* **2009**, *4* (11), 1019–1023.

(20) Wong, T.-S.; Kang, S. H.; Tang, S. K. Y.; Smythe, E. J.; Hatton, B. D.; Grinthal, A.; Aizenberg, J. Bioinspired Self-Repairing Slippery Surfaces with Pressure-Stable Omniphobicity. *Nature* **2011**, *477* (7365), 443–447.
(21) Wang, B. L.; Heng, L.; Jiang, L. Temperature-Responsive Anisotropic Slippery Surface for Smart Control of the Droplet Motion. *ACS Appl. Mater. Interfaces* **2018**, *10* (8), 7442–7450.
(22) Smith, J. D.; Dhiman, R.; Anand, S.; Reza-Garduno, E.; Cohen, R. E.; McKinley, G. H.; Varanasi, K. K. Droplet Mobility on Lubricant-Impregnated Surfaces. *Soft Matter* **2013**, *9* (6), 1772–1780.
(23) Vella, D.; Mahadevan, L. The "Cheerios Effect." *Am. J. Phys.* **2004**, *73* (9), 817–825.
(24) Karpitschka, S.; Pandey, A.; Lubbers, L. A.; Weijs, J. H.; Botto, L.; Das, S.; Andreotti, B.; Snoeijer, J. H. Liquid Drops Attract or Repel by the Inverted Cheerios Effect. *Proc. Natl. Acad. Sci.* **2016**, *113* (27), 7403–7407..
(25) Hui Guan, J.; Ruiz-Gutiérrez, É.; Xu, B. Bin; Wood, D.; McHale, G.; Ledesma-Aguilar, R.; Wells, G. G. Drop Transport and Positioning on Lubricant-Impregnated Surfaces. *Soft Matter* **2017**, *13* (18), 3404–3410.
(26) Geraldi, N. R.; Guan, J. H.; McHale, G.; Fu, Y. Q.; Wells, G. G.; Luo, J. T. Slippery Liquid-Infused Porous Surfaces and Droplet Transportation by Surface Acoustic Waves. *Phys. Rev. Appl.* **2017**, *7* (1).
(27) Bowden, N.; Arias, F.; Deng, T.; Whitesides, G. M. Self-Assembly of Microscale Objects at a Liquid/Liquid Interface through Lateral Capillary Forces. *Langmuir* **2001**, *17* (5), 1757–1765.
(28) Landau, L.; Levich, B. Dragging of a Liquid by a Moving Plate. In *Dynamics of Curved Fronts*; Pelcé, P., Ed.; Academic Press: San Diego, 1988; pp 141–153.
(29) Seiwert, J.; Clanet, C.; Quéré, D. Coating of a Textured Solid. *J. Fluid Mech.* **2011**, *669*, 55–63.
(30) Harkins, W. D.; Feldman, A. Films. The Spreading of Liquids and the Spreading Coefficient. *J. Am. Chem. Soc.* **1922**, *44* (12), 2665–2685.
(31) McHale, G.; Orme, B. V; Wells, G. G.; Ledesma-Aguilar, R. A. Apparent Contact Angles on Lubricant Impregnated Surfaces/SLIPS: From Superhydrophobicity to Electrowetting. *Langmuir* **2019**, *35*.
(32) Banpurkar, A. G.; Nichols, K. P.; Mugele, F. Electrowetting-Based Microdrop Tensiometer. *Langmuir* **2008**, *24* (19), 10549–10551.
(33) Semprebon, C.; McHale, G.; Kusumaatmaja, H. Apparent Contact Angle and Contact Angle Hysteresis on Liquid Infused Surfaces. *Soft Matter* **2017**, *13* (1), 101–110.
(34) Gibbs, J. . The Scientific Papers of J Willard Gibbs. **1906**, *1*.

Table of Contents Graphic

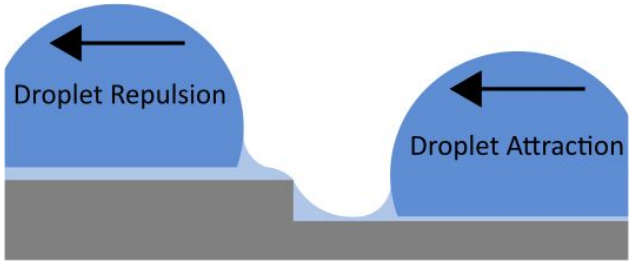

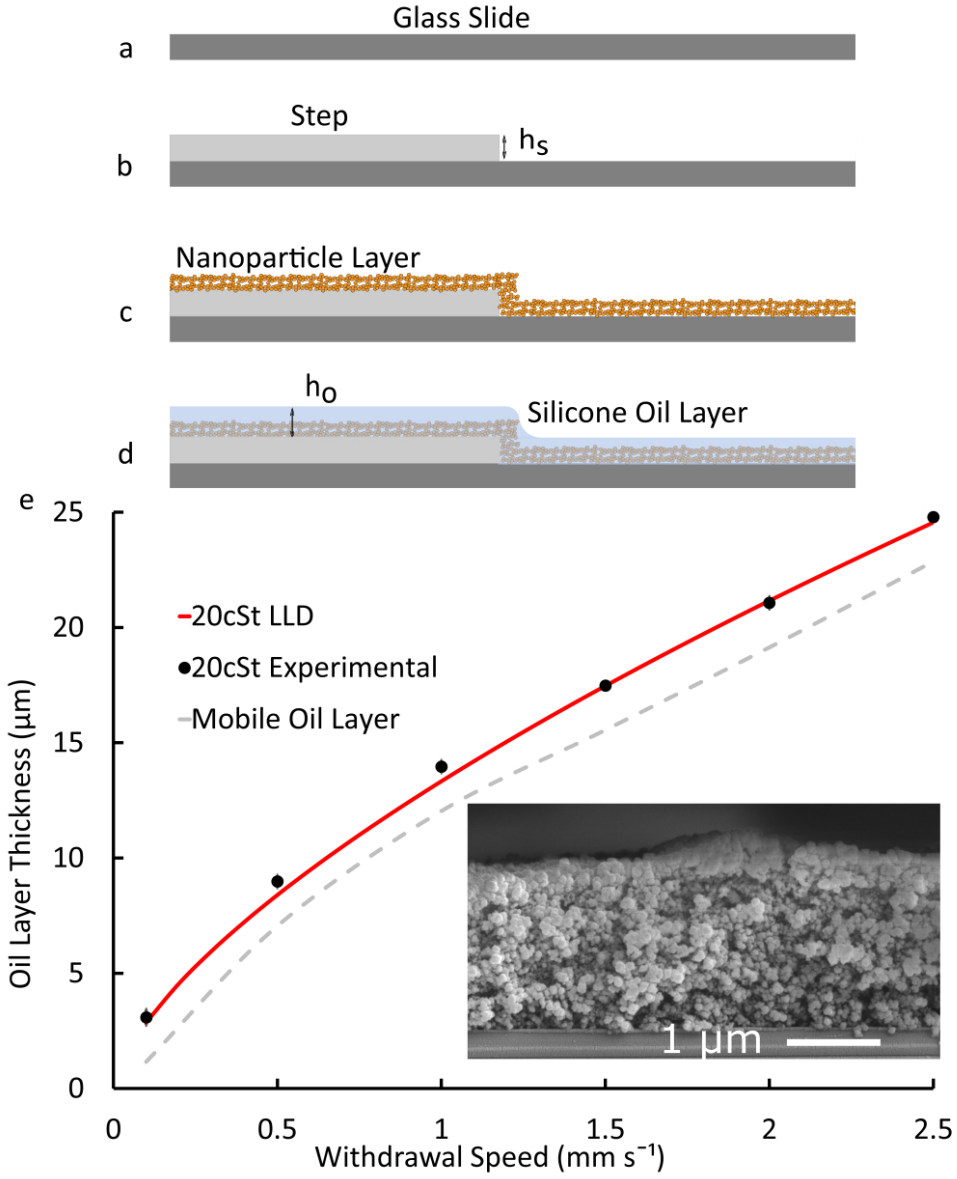

Sample production and characterisation. **a-d** Schematic of the production of the step from, a glass cover slip and SU-8 (via simple photolithography), where h_s is varied and measured by white-light optical profilometry. The nanoparticle coating consists of a commercial product (Glaco) and applied via spray coating. Silicone oil imbibition is performed by a dip coating method where the withdrawal speed can be varied to produce different oil layer thicknesses. **e** SEM image of a typical sample cross section, indicating the uniformity of the coating and nanoparticle layer height. **f** Oil thickness for different withdrawal speeds. Black dots are the experimental layer thickness measured using a reflectometer. Red solid line is a fit to the LLD equation. Grey dashed line indicates the estimated oil layer thickness

86x105mm (300 x 300 DPI)

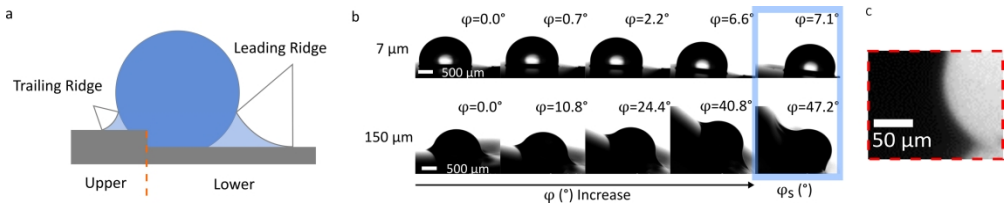

Changes in position and configuration of droplets by varying step height (h_s) and the effect this has on detachment angle (φ_s). **a** A schematic showing how a water droplet interacts with the system with the upper and lower sections designated on the sample and the asymmetry between trailing and leading wetting ridges defined. **b** Sequence of images showing the droplet shape evolution during sample tilting, step detachment and finally droplet motion as h_s increases. **c** In the dashed red box, there is an image at 10 times zoom to depict more clearly the smallest wetting ridge achievable on the thinnest oil layer (h_o= 3.09 µm).

177x35mm (600 x 600 DPI)

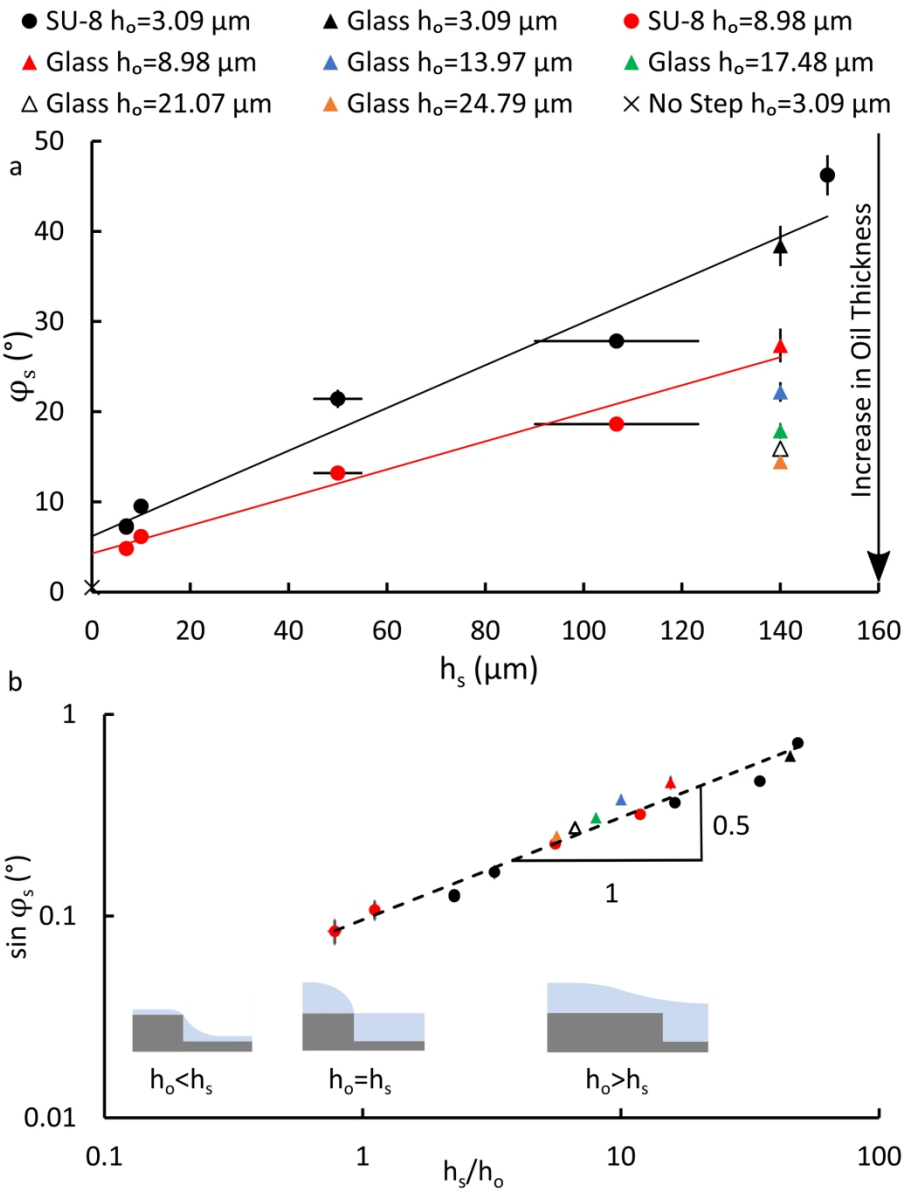

Effect on detachment angle (φ_S) as step height (h_S) increases. **a** Detachment angle (φ_S) data for increasing step heights (black circles and black triangle) for the thinnest oil layer (3.09 µm). Red circles and red triangle show the reduction of φ_S for a thicker oil layer. All triangles indicate the evolution of φ_S from minimum to maximum oil thickness. Each of the data points corresponds to an average of five experimental results. **b** Data from **a** plotted on a log-log scale with accompanying oil layer schematics. sin(φ$_S$) scales as the square root of the ratio of step height to oil thickness.

85x113mm (600 x 600 DPI)

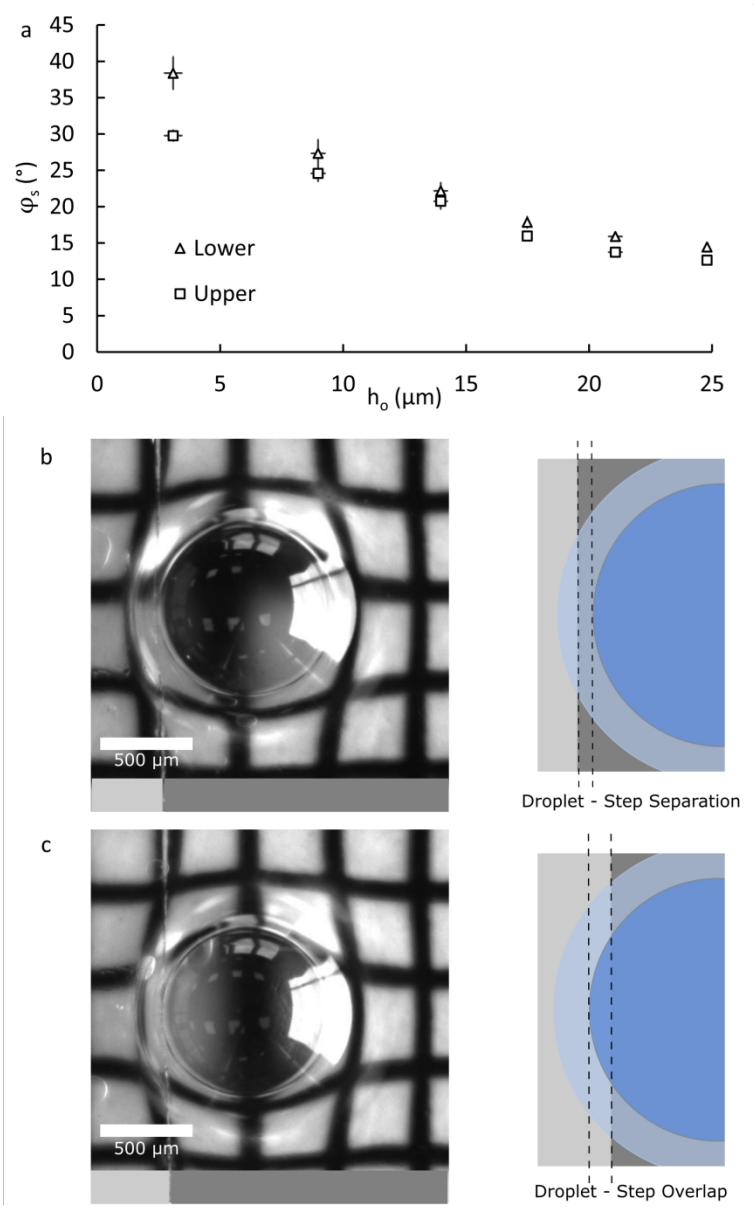

Exact droplet positions when droplet has arrived at its final stationary point on the stepped samples, close to the point of detachment, given differing initial positions. **a** Detachment angles for 140 µm h_S with increasing oil layer thickness. Squares initial position on the step's upper portion, triangles on the lower, both tilted in a clockwise direction (away from the step). **b** Top view of 2 µl droplet close to step detachment, with its initial position having been on the upper portion of the step, along with a schematic to show the droplets separation from the step. **c** 2 µl droplet close to step detachment where the droplets initial position was on the lower portion of the stepped sample. The accompanying schematic indicates the droplets overlap with the step.

86x137mm (600 x 600 DPI)

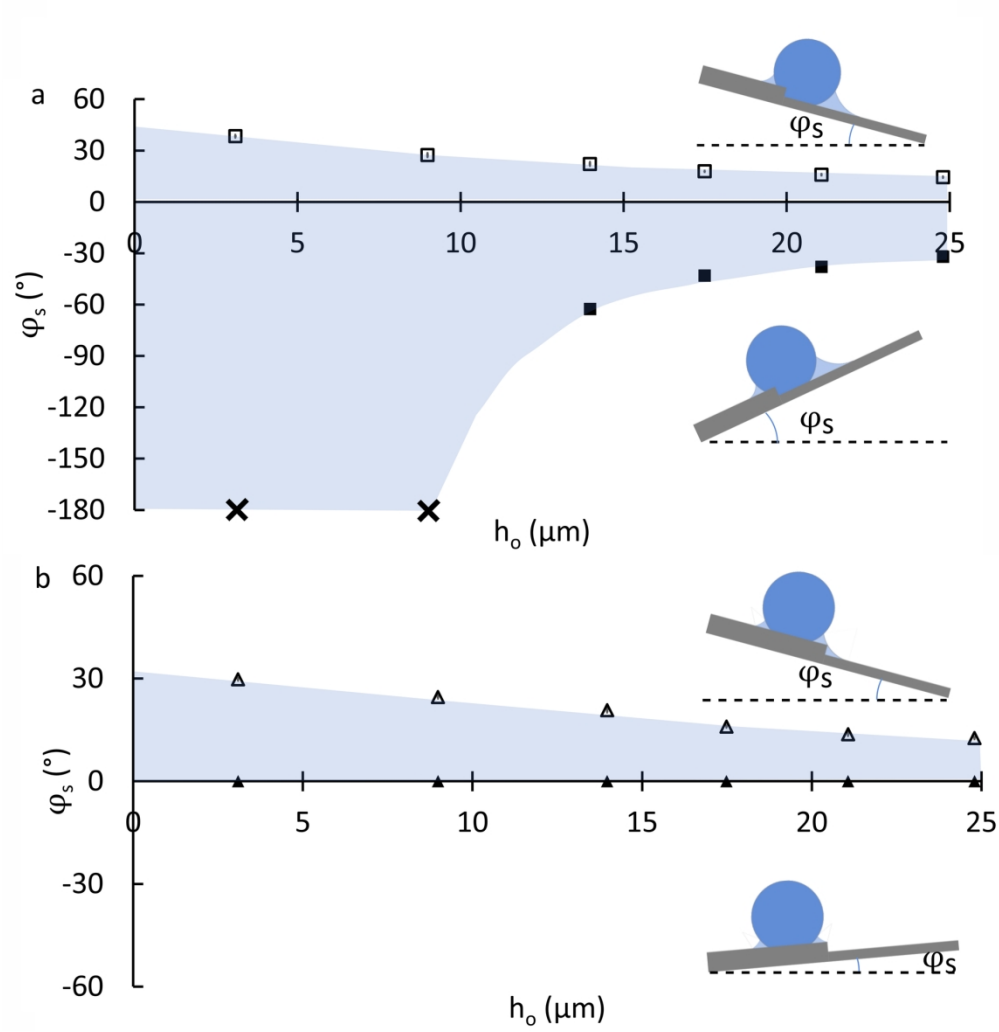

Changes in droplets initial position and direction of tilt (clockwise/anticlockwise). **a** Comparison between 2 µl droplets placed on the lower portion of the step and tilted both clockwise and anticlockwise for increasing oil thickness. Shaded area indicates where the droplet is stationary on the surface and stuck to the step. The (crosses) indicate droplets that did not slide at all on the surface and remained there even at 180°. **b** 2 µl droplet placed on the upper portion of the step and the same procedure as seen in a applied. The error bars on both graphs are equivalent to the size of the symbols and each data point corresponds to an average of results from 5 experiments.

85x88mm (600 x 600 DPI)

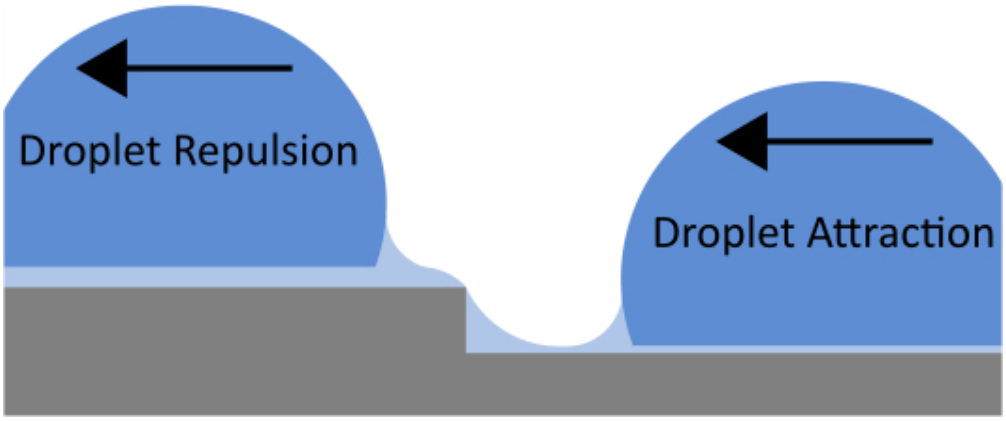

149x61mm (90 x 90 DPI)